arXiv:2211.00927v2 [cond-mat.soft] 9 Nov 2022

Transport of ions in hydrophobic nanotubes

Olga I. Vinogradova,[1,*] Elena F. Silkina,[1] and Evgeny S. Asmolov[1]

[1] *Frumkin Institute of Physical Chemistry and Electrochemistry, Russian Academy of Sciences, 31 Leninsky Prospect, 119071 Moscow, Russia*

(Dated: November 10, 2022)

The theory of electrokinetic ion transport in cylindrical channels of a fixed surface charge density is revisited. Attention is focused on impact of the hydrophobic slippage and mobility of adsorbed surface charges. We formulate generalised Onsager relations for a cylinder of an arbitrary radius and then derive exact expressions for the mean electro-osmotic mobility and conductivity. To employ these expressions we perform additional electrostatic calculations, with the special focus on the non-linear electrostatic effects. Our theory provides a simple explanation of a giant enhancement of the electrokinetic mobility and conductivity of hydrophobic nanotubes by highlighting the role of appropriate electrostatic and hydrodynamic length scales and their ratios. We also propose a novel interpretation of zeta potentials of cylindrical channels.

I. INTRODUCTION

Nanopores are ubiquitous to nature, and nanoporous materials found applications in various technologies. Electrokinetic transport phenomena in nanotubes include an electro-osmotic flow in response to an applied electric field, a conductance, emerging due to a convective ion transfer by this flow in addition to a conventional migration of ions (electrophoresis), and also a streaming current that is generated by pressure gradient if any [1, 2]. The transport of ions (i.e. streaming and conductivity currents) in these nanoscale systems is of especial interest being important for physiological phenomena, energy harvesting, biosensing and more [3–7]. Besides, from the measured streaming current the zeta potential of surfaces can be inferred, which is important in colloid and interface science [8–10]. Finally, with the advent of nanofluidics there has been considerable interest in an unusually high conductance of electrolyte solutions in confined systems.

Extensive efforts have gone into investigating conductivity in nanotubes and flat-parallel slits experimentally. Stein *et al.* [11] found a remarkably high conductivity of dilute solutions in nanoslits that is independent on the salt concentration. The corresponding to a saturation plateau conductivity augments with the surface charge density [12]. Measurements in nanotubes have shown that the conductivity plateau decreases with the radius [13]. Balme *et al.* [14] reported that the height of conductance plateaus is augmented in hydrophobic nanopores. The body of experimental work investigating the streaming current (including inferring the zeta potential) is much less than that for the conductivity current, although there is some literature in this area [15–18]. However, despite a rapid rise of an experimental activity, ion transport has been given insufficient attention compared with the transport of water. For example, we are unaware of any previous work that has addressed the impact of hydrodynamic (hydrophobic) slippage [19–24] on the streaming current, although the amplification of an electro-osmotic flow in slippery channels was a subject of active experimental research [25–28].

There is some literature describing attempts to provide a satisfactory theory of electric currents emerging in confined electrolytes. The majority of previous work considered planar geometries (where the exact solution to a non-linear electrostatic problem exists, although can only be expressed in terms of an elliptic integral) and assumed the classical no-slip boundary conditions at the charged walls [29]. The conductivity plateau at low salt has been attributed to the surfaces of a constant charge density [11]. Bocquet and Charlaix [2] have briefly discussed the expected shift of the conductance plateau due to a hydrodynamic slip, assuming immobile surface charges. Applying some simple scaling arguments these authors propose that this should be $\propto b/\ell_{GC}$, where b is the slip lenth and ℓ_{GC} is the Gouy-Chapman length, which is inversely proportional to the surface charge density [30]. At slippery surfaces adsorbed charges could be mobile, and, therefore, responding to the external electric field as discussed by Maduar *et al.* [31] and supported by *ab initio* simulations [32]. Mouterde and Bocquet [33] derived scaling expressions describing a contribution of a hydrodynamic slip taking into account the mobility of adsorbed ions that later allowed one to interpret the computer simulation data on channel conductivity with physisorbed surface charges [34]. Their results, however, apply only for a situation of channels of a thickness that significantly exceeds the Debye length λ_D of the bulk electrolyte. Recently Vinogradova *et al.* [35] proposed an analytical theory of ion conductivity in slippery parallel-plate channels of an arbitrary thickness. These authors derived simple expressions for the mean conductivity of the channel in two regimes, of thick and thin slits, highlighting the role of hydrodynamic slip and mobility of adsorbed surface charges.

Cylinders constitute a more realistic model for artificial nanotubes and real porous materials, but remain much less theoretically understood. The main challenge is related to electrostatic calculations in the cylindrical geometry. Since the exact solution to non-linear electrostatic problem is still unknown, one needs to rely on numerical solutions or approximations. The analytical theory of an electro-osmotic flow in no-slip nanotubes developed by Rice and Whitehead [36] is restricted to small surface potentials. Later Levine *et al.* [37] extended this model for a no-slip cylinder to higher potentials and obtained expressions for streaming and conductivity cur-

* Corresponding author: oivinograd@yahoo.com

rents, but only in the integral form. During last few years some approximate analytical expressions for a conductance in cylindrical nanopores have been obtained by postulating either the overall electroneutrality ('Donnan equilibrium') [38, 39], and also for the 'counter-ions only' case (so-called co-ion exclusion approximation) [40]. A slippery nanotube has been considered in [41]. These authors proposed an expression relating the conductivity to the integral of an electrostatic potential, assuming the surface charges are immobile. Numerical integration showed that at a given (high) surface charge the conductivity increases with the slip length, but a physical interpretation of this result has not been proposed. Green [42] also studied hydrophobic nanotubes with immobile surface charged and derived some useful expressions for transport coefficients. He showed that the hydrodynamic slip boundary conditions are consistent with the Onsager relations. Silkina *et al.* [43] performed calculations of an electro-osmotic flow in nanotubes by applying electro-hydrodynamic slip boundary conditions [31], i.e. allowing for a mobility of adsorbed charges in response to electric field. They obtained a rigorous asymptotic result for a situation of strongly overlapping diffuse layers at high surface potential and predicted a parabolic velocity (and potential) profile. This solution, however, is accurate only when $\lambda_D/\ell_{GC} \leq 1$, i.e. when the surface charge is sufficiently small. The authors interpreted the shift (amplification) of the electro-osmotic velocity profile due to slippage and concluded that the mobility of adsorbed charges reduces the effect, but made no attempt to investigate the transport of ions.

In this paper we present the results of a study of ion transport in the hydrophobic nanotubes with the fixed surface charge density. The hydrophobicity implies that the electro-hydrodynamic boundary condition [31] is imposed, i.e. besides hydrophobic slippage we deal with a migration of adsorbed ions in response to an applied electric field. The theory has the merit of yielding useful analytical results as well as being very well suited to numerical work. Our work provides new insight into streaming and conductivity currents in the nanotubes, as well as gives an interpretation of their zeta potential.

Our paper is arranged as follows. In Sec. II, we define our system and present some general considerations concerning the Onsager relations and transport coefficients. Section II A describes the derivation of the Onsager relations for a hydrophobic nanotube. A detailed calculation of coefficients for the mobility matrix is presented in Sec. II B. The concept of a zeta potential of hydrophobic nanotubes is introduced. The approximate equations for zeta potentials and mean conductivity are derived in Sec. III. Numerical results for zeta-potentials and conductivity are presented in Sec. IV and compared with approximate theoretical expressions. We conclude in Sec. V. In Appendix A we briefly discuss the possible reduction of ion mobilities with salt concentration to argue that this effect can safely be neglected in our system. Appendix B contains a derivation of electrostatic relationships required for calculations of streaming and conductivity currents.

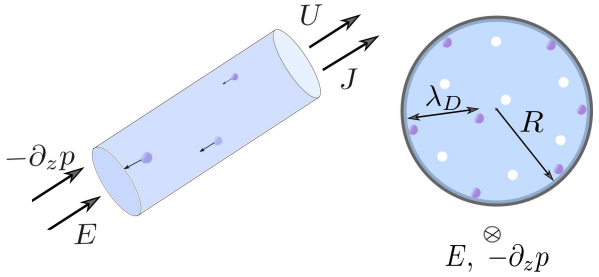

FIG. 1. Sketch of the charged nanotube of radius R that is coupled with a bulk electrolyte reservoir characterized by the Debye length λ_D. An applied pressure gradient $-\partial_z p$ induces a hydrodynamic flow and streaming current. An applied electric field E induces an electro-osmotic velocity and a conductivity current. The confined electrolyte flows with the mean velocity U and has the mean current density J.

II. GENERAL THEORY

We consider an 1:1 aqueous electrolyte solution of a dynamic viscosity η and permittivity ε in contact with a charged nanotube of radius R as sketched in Fig. 1. The local number density (per unit volume) of cations and anions are n_+ and n_-, respectively, and, therefore, the charge densities at each point are $\rho_\pm = en_\pm$, where e is the elementary positive charge. Defining n_∞ as the number density in the bulk one can write for the Boltzmann distribution of density $n_\pm(r) = n_\infty \exp(\mp\phi(r))$, where $\phi(r) = e\Phi(r)/(k_B T)$ is the dimensionless electrostatic potential, where k_B is the Boltzmann constant, T is a temperature of the system.

The cylindrical system (z,r) of coordinates is defined, such that z coincides with the axis of the nanotube, and r is the radial axis. The surface of nanotube is thus located at $r = R$ and we denote its potential as Φ_s and a charge density as σ. Without loss of generality, the surface charges are taken as cations (σ is positive).

A. Onsager relations

In the general case, the nanotube subject to a pressure gradient $\partial_z p$ and an electric field E in the z direction. Thus the flow inside the nanotube satisfies the Stokes equation, which includes an electrostatic body force $E\rho$

$$\eta\nabla^2 u = \partial_z p + E\rho, \tag{1}$$

where $\nabla^2 = \partial_r^2 + r^{-1}\partial_r$ for the cylindrical geometry, $u(r)$ is the fluid velocity and ρ is the total charge density at each point r. It follows from the Poisson equation that

$$E\rho = -E\frac{\varepsilon\nabla^2\Phi}{4\pi}. \tag{2}$$

Note that CGS (Gaussian) electrostatic units are used throughout our paper. However, by expressing all characteristic lengths in terms of the introduced below Bjerrum and Debye lengths we will obtain the results that are independent of any specific system of units.

If the bulk reservoir represents a 1:1 salt solution of concentration c_∞, then

$$E\rho = -E\frac{\varepsilon k_B T \nabla^2 \phi}{4\pi e} = -\frac{eE\nabla^2\phi}{4\pi\ell_B}, \tag{3}$$

where $\ell_B = \dfrac{e^2}{\varepsilon k_B T}$ is the Bjerrum length. Note that ℓ_B of water is equal to about 0.7 nm for room temperature.

Consequently, Eq.(1) can be rewritten as

$$\eta\nabla^2 u = \partial_z p + \frac{eE}{4\pi\ell_B}\nabla^2\phi \tag{4}$$

We assume weak field, so that in steady state $\phi(r)$ is independent on the fluid flow and satisfies the nonlinear Poisson-Boltzmann equation

$$\nabla^2\phi = \frac{1}{r}\frac{d}{dr}\left(r\frac{d\phi}{dr}\right) = \lambda_D^{-2}\sinh\phi \tag{5}$$

where $\lambda_D = (8\pi\ell_B n_\infty)^{-1/2}$ is the Debye screening length of an electrolyte solution. Note that by analysing the experimental data it is more convenient to use the concentration c_∞[mol/L], which is related to n_∞[m^{-3}] as $n_\infty = N_A \times 10^3 \times c_\infty$, where N_A is Avogadro's number. We also recall that a useful formula for 1:1 electrolyte is [44]

$$\lambda_D[\text{nm}] = \frac{0.305[\text{nm}]}{\sqrt{c_\infty}[\text{mol/L}]}, \tag{6}$$

so that upon increasing c_∞ from 10^{-7} (in pure water, where the ionic strength is due to the dissociating H^+ and OH^- ions) to 10^{-1} mol/L the screening length is reduced from about 1 μm down to ca. 1 nm.

To integrate Eq.(5) we impose two electrostatic boundary conditions. The first condition always reflects the symmetry of the channel $\phi'|_{r=0} = 0$, where $'$ denotes d/dr. The second condition is applied at the walls and can be either that of a constant surface potential (conductors) or of a constant surface charge density (insulators). Here we limit ourselves by the constant charge condition, which can be formulated as

$$\phi'|_{r=R} = \frac{2}{\ell_{GC}}, \tag{7}$$

where $\ell_{GC} = \dfrac{e}{2\pi\sigma\ell_B}$ is the Gouy-Chapman length. For high surface charges, say $\sigma \simeq 36$ mC/m^2, the Gouy-Chapman length is small, $\ell_{GC} \simeq 1$ nm. However, $\sigma \simeq 0.73$ mC/m^2 gives $\ell_{GC} \simeq 50$ nm.

The linearity of Eq.(4) implies that its solution represents the decoupled and superimposed contribution of the pressure-driven and electro-osmotic flows

$$u = -m_h\partial_z p + m_e E, \tag{8}$$

where m_h and m_e are the functions of r that depend on electrostatic and electro-hydrodynamic boundary conditions at the solid wall. Below we refer these functions to as hydrodynamic and electro-osmotic mobilities. Note that the first term in (8) is taken with minus to provide positive m_h when $\partial_z p < 0$. As we will see below, a sign of m_e depends on the sign of the surface charge (potential).

It is convenient to use the average values of variables, $U = \overline{u}$, $M_h = \overline{m_h}$, and $M_e = \overline{m_e}$. For any variable f its average value across the cross-section of the cylindrical nanotube is given by

$$\overline{f} = \frac{2}{R^2}\int_0^R rf dr. \tag{9}$$

Formally the above considerations are equivalent to the statement that in the linear response regime, the transport of water and ions through the nanotube can be then expressed in terms of mobility matrix $\mathscr{M}$:

$$\begin{pmatrix} U \\ J \end{pmatrix} = \begin{pmatrix} M_h & M_e \\ M_e & K \end{pmatrix}\begin{pmatrix} -\partial_z p \\ E \end{pmatrix} = \mathscr{M}\begin{pmatrix} -\partial_z p \\ E \end{pmatrix} \tag{10}$$

where J [A/m^2] is the mean current density

$$J = \overline{j} + J_\sigma, \tag{11}$$

and K [S/m] is the mean conductivity of the channel. The first term in (11) is associated with the transport of the diffuse cations and anions inside the nanotube that generates the local density of current $j = j_+ + j_-$. The second term reflects the contribution of the surface current j_σ emerging due to adsorbed mobile ions that are located at the ring of perimeter $2\pi R$. Therefore, this surface averaged contribution to the mean current density is given by $J_\sigma = 2j_\sigma/R$.

As a side note, in experiment one usually measure the conductance G [S]. For a nanotube of length L

$$G = K\frac{\pi R^2}{L} \tag{12}$$

A 2×2 mobility matrix $\mathscr{M}$ is expected to be positive definite and symmetric (with equal off-diagonal coefficients), as assumed in (10), by analogy with Onsager's relations in (bulk) non-equilibrium thermodynamics. The consequence of the symmetry is so-called electrohydrodynamic coupling

$$\frac{J}{-\partial_z p}|_{E=0} = \frac{U}{E}|_{-\partial_z p=0}. \tag{13}$$

The mobility matrix $\mathscr{M}$ fully characterizes electrokinetic phenomena in the nanotubes and, once its elements are known, Eq.(10) can be used to find, without tedious calculations, the liquid flows and currents that are generated by any combination of two applied forces.

However, it is by no means not obvious that by imposing appropriate for hydrophobic surfaces electro-hydrodynamic boundary conditions, Eq.(10) will necessarily hold. More precisely, the equality of off-diagonal elements M_e is still an assumption that should be proven for a situation when the fluid velocity at $r = R$ satisfies [31]

$$u|_{r=R} = b\left(-\partial_r u|_{r=R} + \frac{(1-\mu)eE}{2\pi\eta\ell_B\ell_{GC}}\right) \tag{14}$$

The parameter μ is the fraction of immobile surface charges that can vary from 0 for fully mobile charges to 1 in the case when all adsorbed ions are fixed. The hydrodynamic slip length b in (14) can be of the order of several tens of nanometers [21–24], but not much more. In our calculations we use $b = 10$ nm. However, our discussion will also include a larger value of $b = 100$ nm reported in experiment [24].

To prove the consistency of Eq.(14) with the Onsager relations we have to calculate the coefficients of the mobility matrix. In doing so it is convenient to set one of two possible driving forces to zero.

B. Coefficients of the mobility matrix $\mathscr{M}$

1. Pressure-driven flow

If $E = 0$, Eq. (10) reduces to

$$\begin{pmatrix} U \\ J \end{pmatrix} = \begin{pmatrix} M_h & M_e \\ M_e & K \end{pmatrix} \begin{pmatrix} -\partial_z p \\ 0 \end{pmatrix} = -\partial_z p \begin{pmatrix} M_h \\ M_e, \end{pmatrix} \tag{15}$$

i.e. $U = -M_h \partial_z p$ (Poiseuille's law), and $J = -M_e \partial_z p$. In other words, an applied pressure gradient induces not only a hydrodynamic flow, but also an electric current, which is traditionally termed a streaming current.

Local mobilities can be obtained by integrating Eq. (4) without an electric body force. The boundary condition (14) reduces to a classical hydrodynamic slip boundary condition, and second condition is naturally $\partial_r u(r)|_{r=0} = 0$. This gives for a velocity of the pressure-driven flow

$$u = -\frac{R^2}{4\eta}\left[1 - \frac{r^2}{R^2} + \frac{2b}{R}\right]\partial_z p \tag{16}$$

The local and mean hydrodynamic mobilities are, therefore,

$$m_h = \frac{R^2}{4\eta}\left[1 - \frac{r^2}{R^2} + \frac{2b}{R}\right], M_h = \frac{R^2}{8\eta}\left(1 + \frac{4b}{R}\right) \tag{17}$$

The local densities of current due to diffuse ions are $j_\pm = \pm e n_\pm u$ with u given by (16). Consequently,

$$\overline{j_\pm} = \pm \frac{2en_\infty}{R^2}\int_0^R r e^{\mp\phi} u dr \tag{18}$$

Summing up these functions and using the Poisson-Boltzmann equation (5), we conclude that the contribution of the diffuse ions to the density of current can be obtained by taking the integral

$$\overline{j} = -\frac{4en_\infty\lambda_D^2}{R^2}\int_0^R r u \nabla^2\phi dr \tag{19}$$

Performing (twice) standard integration by parts we then obtain

$$\overline{j} = -\frac{e}{4\pi\eta\ell_B}\partial_z p\left[\overline{\phi} - \phi_s - \frac{2b}{\ell_{GC}}\right] \tag{20}$$

If the adsorbed mobile ions are transferred along the wall with the slip velocity of liquid $u(R) = -\frac{bR}{2\eta}\partial_z p$, then they generate the surface current density

$$j_\sigma = \sigma(1-\mu)u(R) = -\frac{e(1-\mu)bR}{4\pi\eta\ell_{GC}\ell_B}\partial_z p, \tag{21}$$

whence

$$J_\sigma = -\frac{e(1-\mu)b}{2\pi\eta\ell_{GC}\ell_B}\partial_z p \tag{22}$$

Substituting Eqs.(20) and (22) into (11) we derive for the mean streaming current density

$$J = -\frac{e}{4\pi\eta\ell_B}\left(\overline{\phi} - \phi_s - \frac{2\mu b}{\ell_{GC}}\right)\partial_z p \tag{23}$$

The corresponding mean electro-osmotic mobility is

$$M_e = \frac{e}{4\pi\eta\ell_B}\left(\overline{\phi} - \phi_s - \frac{2\mu b}{\ell_{GC}}\right) = -\frac{e}{4\pi\eta\ell_B}\zeta \tag{24}$$

The new dimensionless parameter ζ introduced above can be termed a (dimensionless) electro-hydrodynamic or zeta potential

$$\zeta = \zeta_0 + \Delta\zeta, \tag{25}$$

where

$$\zeta_0 = \phi_s - \overline{\phi} \tag{26}$$

is expected for a hydrophilic nanotube and associated with the (sensitive to amount of added salt) electrostatic contribution, and

$$\Delta\zeta = \frac{2\mu b}{\ell_{GC}} \tag{27}$$

is associated with the slip-driven contribution that does not depend on the salt concentration.

Note that if we postulate the no-slip boundary condition ($b = 0$) and assume that the capillary is infinitely thick (which is equivalent to $\overline{\phi} \to 0$), Eq. (25) predicts that ζ must be equal to the surface potential. However, in the case of slippery nanotubes the situation is more complicated and ζ does not solely reflect ϕ_s, but also depends on the finite average potential in the nanotube and on the charged wall slippage properties. We shall return to this issue later.

2. Electro-osmotic flow

If $\partial_z p = 0$, one can reduce Eq. (10) to

$$\begin{pmatrix} U \\ J \end{pmatrix} = \begin{pmatrix} M_h & M_e \\ M_e & K \end{pmatrix} \begin{pmatrix} 0 \\ E \end{pmatrix} = E \begin{pmatrix} M_e \\ K \end{pmatrix}, \tag{28}$$

which indicates that an applied electric field E induces both an electro-osmotic flow with the average velocity $U = M_e E$

and an electric current of mean density $J = KE$ (Ohm's law). This current is referred below to as a conductivity current.

The electro-osmotic velocity is obtained by integrating Eq. (4) with prescribed boundary conditions (of symmetry and Eq.(14))

$$u = \frac{eE}{4\pi\eta\ell_B}\left[\phi - \phi_s - \frac{2\mu b}{\ell_{GC}}\right], \tag{29}$$

whence the local electro-osmotic mobility is

$$m_e = \frac{e}{4\pi\eta\ell_B}\left[\phi - \phi_s - \frac{2\mu b}{\ell_{GC}}\right] \tag{30}$$

and consequently, M_e is again expressed by Eq.(24). This result provides a proof of Onsager relations (10) if boundary condition (14) are applied. We stress, however, that to satisfy the Onsager relations the condition (21) for the surface current density should necessary supplement Eq.(14).

The mean density of the emerging conductivity current is given by Eq.(11), but besides a convective transfer with the fluid velocity that is now described by Eq.(29), ions migrate under an applied field, i.e. they also move relative to a fluid.

The velocity of diffuse ions is thus $\mathscr{U}_\pm = u \pm m_\pm E$, where u is the velocity of the electro-osmotic flow given by (29) and $m_\pm$ is the (electrophoretic) mobility of ions. To keep calculations as transparent as possible we set $m_\pm = m = e/(6\pi\eta\mathscr{R})$, where $\mathscr{R}$ is the hydrodynamic radius of both cations and anions (in calculations below we will use $\mathscr{R} = 0.3$ nm). In such a definition m is treated as equal to the ion mobility at zero ionic strength and we neglect its the possible (weak with our parameters) reduction on increasing n_∞ (see Appendix A). If so,

$$\overline{j_\pm} = \pm\frac{2en_\infty}{R^2}\int_0^R e^{\mp\phi}(u \pm m_\pm E)rdr \tag{31}$$

and consequently

$$\overline{j} = \frac{4en_\infty}{R^2}\int_0^R r\left(-u\sinh\phi + \frac{eE}{6\pi\eta\mathscr{R}}\cosh\phi\right)dr, \tag{32}$$

which is equivalent to

$$\overline{j} = K_\infty E\left[-\frac{3\lambda_D^2\mathscr{R}}{\ell_B R^2}\int_0^R m_e\nabla^2\phi rdr + \overline{\cosh\phi}\right], \tag{33}$$

where

$$K_\infty = \frac{e^2 n_\infty}{3\pi\eta\mathscr{R}}, \tag{34}$$

is the conductivity of the bulk electrolyte solution.

Substituting expression (30) for m_e and integrating twice by parts we obtain

$$\overline{j} = K_\infty E\left[\overline{\cosh\phi} + \frac{3\lambda_D^2\mathscr{R}\overline{(\phi')^2}}{2\ell_B} + \frac{12\mu b\lambda_D^2\mathscr{R}}{R\ell_{GC}^2\ell_B}\right] \tag{35}$$

The adsorbed mobile ions generate the density of current

$$\begin{aligned} j_\sigma &= \sigma(1-\mu)[u(R) + mE] \\ &= \frac{(1-\mu)e}{2\pi\ell_{GC}\ell_B}\left(-\frac{eE}{2\pi\eta\ell_B}\frac{\mu b}{\ell_{GC}} + \frac{eE}{6\pi\eta\mathscr{R}}\right), \end{aligned} \tag{36}$$

where we have substituted $u(R) = -\dfrac{eE\mu b}{2\pi\eta\ell_B\ell_{GC}}$. Standard manipulations lead to

$$J_\sigma = K_\infty E\left(\frac{4\lambda_D^2(1-\mu)}{\ell_{GC}} - \frac{12\mathscr{R}(1-\mu)\lambda_D^2\mu b}{\ell_{GC}^2\ell_B}\right) \tag{37}$$

Summing up Eqs.(35) and (37) we find the mean density of the conductivity current J, and then by dividing it by E obtain the expression for the mean conductivity

$$K = K_\infty\left[\overline{\cosh\phi} + \frac{3\lambda_D^2\mathscr{R}\overline{(\phi')^2}}{2\ell_B} + \frac{4\ell_{Du}}{R}\left(\frac{3\mathscr{R}\mu^2 b}{\ell_{GC}\ell_B} + 1 - \mu\right)\right], \tag{38}$$

where we use another electrostatic length scale

$$\ell_{Du} = \frac{\lambda_D^2}{\ell_{GC}} \tag{39}$$

termed the Dukhin length. Note that ℓ_{Du} can be larger than any conceivable Debye length. For example, the values of $\lambda_D = 50$ nm and $\ell_{GC} = 2$ nm lead to $\ell_{Du} = 1.25$ μm, which for a nanotube of $R = 10$ nm gives $\ell_{Du}/R = 125$.

It is convenient to divide the mean conductivity of the channel given by (38) into a "no-slip" conductivity K_0 expected for hydrophilic channels, and slip-driven contribution ΔK:

$$K = K_0 + \Delta K, \tag{40}$$

where

$$K_0 = K_\infty\left[\frac{3\lambda_D^2\mathscr{R}\overline{(\phi')^2}}{2\ell_B} + \overline{\cosh\phi}\right], \tag{41}$$

and

$$\Delta K = K_\infty\frac{4\ell_{Du}}{R}\left[\frac{3\mu^2 b}{\ell_{GC}}\frac{\mathscr{R}}{\ell_B} + 1 - \mu\right]. \tag{42}$$

Equation (41) is equivalent to the formula for K_0 of a plate-parallel channel [35]. However, now $\overline{(\phi')^2}$ and $\overline{\cosh\phi}$ should be calculated for a cylindrical geometry. The form of Eq.(42) is identical to that for ΔK of a plate-parallel channel [35]. The only difference is that Eq.(42) includes the nanotube radius R instead of the channel thickness.

III. APPROXIMATE SOLUTIONS

In the previous section we have proven the Onsager relations and obtained the general equations for the mean electro-osmotic mobility and the mean conductivity of the nanotube. In order to employ them a detailed information concerning mean electrostatic parameters, such as $\overline{\phi}$, $\overline{\cosh\phi}$, etc, is required. The derivation of equations that determine them is given in Appendix B.

A. Electro-osmotic mobility and zeta potential

From Eq. (24) it follows that to calculate the electro-osmotic mobility it is enough to find the zeta potential, which incorporates all geometry and electrostatic parameters of the problem.

For a thick cylinder, Eq.(B4) for ϕ_s of isolated surface remains accurate. Substituting this equation into (26) and making the additional assumption that $\overline{\phi} \simeq 0$ one obtains

$$\zeta_0 \simeq 2\,\mathrm{arsinh}(\frac{\lambda_D}{\ell_{GC}}) \tag{43}$$

An approximate ζ_0 given by Eq.(43) may slightly overestimate the exact value since in the cylinder of finite R the average potential does not vanish in the general case (see Appendix B). For weakly charged surface Eq.(43) reduces to

$$\zeta_0 \simeq \frac{2\lambda_D}{\ell_{GC}} \tag{44}$$

All together, ζ_0 of a thick cylinder always depends on salt concentration, and is approximately equal to ϕ_s.

In the thin-channel regime, substituting (B13) and (B14) into Eq.(26) we derive

$$\zeta_0 \simeq \frac{R}{2\ell_{GC}} \tag{45}$$

Thus, ζ_0 of a thin nanotube is not equal to ϕ_s given by (B13) and depends only on the surface charge and the nanotube radius. Importantly, the zeta potential of a thin hydrophilic cylinder does not depend on the salt concentration, although ϕ_s given by (B13) reduces on increasing c_∞.

The additional slip-driven contribution $\Delta\zeta$ in Eq.(25) does not depend on salt and is of the same form for a cylinder of any thickness and is given by Eq.(27). It is instructive to calculate the relative enhancement of zeta potential $\zeta/\zeta_0 = 1+\Delta\zeta/\zeta_0$ due to slippage. Say, straightforward calculations give for a thick cylinder

$$\frac{\zeta}{\zeta_0} \simeq 1 + \frac{\mu b}{\ell_{GC}\,\mathrm{arsinh}(\frac{\lambda_D}{\ell_{GC}})} \tag{46}$$

When the nanotube is weakly charged, Eq. (46) reduces to

$$\frac{\zeta}{\zeta_0} \simeq 1 + \frac{\mu b}{\lambda_D}, \tag{47}$$

which indicates that an enhancement of zeta potential can become very large at high salt.

For a thin cylinder

$$\frac{\zeta}{\zeta_0} \simeq 1 + \frac{4\mu b}{R} \tag{48}$$

is defined only by the ratio $\mu b/R$ and does not depend on salt. To give an idea on possible zeta potential enhancement, with $\mu b = 100$ nm and $R = 10$ nm, we get ca. 40 times amplification!

B. Conductivity

The substitution of Eqs.(B9) and (B10) into Eq. (41) allows one to immediately obtain an expression for electrical conductivity in the thick hydrophilic cylinder

$$K_0 \simeq K_\infty \left[1 + \frac{4\lambda_D}{R}\left(\sqrt{1+\frac{\ell_{Du}}{\ell_{GC}}} - 1\right)\left(1 + \frac{3\mathscr{R}}{\ell_B}\right)\right]. \tag{49}$$

In the thin-channel regime, $\overline{\cosh\phi}$ and $\overline{(\phi')^2}$ are given by Eqs.(B16) and (B15), respectively. Substituting them to (41) we derive

$$K_0 \simeq K_\infty \left[\sqrt{1+\left(\frac{4\ell_{Du}}{R}\right)^2} - \frac{2\ell_{Du}}{\ell_{GC}}\left(1 - \frac{3\mathscr{R}}{2\ell_B}\right)\right], \tag{50}$$

where the first term is of the leading-order. The significant deviations from the bulk conductivity are expected when $\ell_{Du}/R \geq 1$. In this case K_0 does not depend on c_∞:

$$K_0 \simeq K_\infty \frac{4\ell_{Du}}{R} \tag{51}$$

In other words, the salt dependence of K_0 should demonstrate a conductivity plateau in dilute solutions.

In the case of hydrophobic channels the conductivity can be obtained from Eq. (40), i.e. by summing up the corresponding K_0 and ΔK given by (42). The conductivity amplification due to slippage, $K/K_0 = 1+\Delta K/K_0$, can then be easily found. For example, if $\ell_{Du}/R \geq 1$ and λ_D/ℓ_{GC} is small enough, i.e. in the thin channel regime, it follows from Eq. (51) that

$$\frac{K}{K_0} \simeq \frac{3\mu^2 b}{\ell_{GC}}\frac{\mathscr{R}}{\ell_B} + 2 - \mu, \tag{52}$$

indicating that the enhancement compared to a hydrophilic nanotube can be very large, a few tens of times, provided ℓ_{GC} is small (highly charged surfaces) and adsorbed charges are immobile ($\mu = 1$). Interestingly, $K/K_0 = 2$ when $\mu = 0$, i.e. with fully mobile surface charges the mean conductivity remains enhanced compared to that in hydrophilic nanotube. We recall that in this situation the electro-osmotic flow is the same as in a hydrophilic nanotube.

IV. RESULTS AND DISCUSSION

In order to assess the validity of the above analysis, we perform a numerical resolution of Eq.(5) complemented by the boundary condition (7) following the numerical approach developed by Bader and Asche. Once ϕ and corresponding average functions are found numerically (see Appendix A), the streaming and conductivity currents, zeta potential and mean conductivity can be obtained using the expressions derived in Sec. II and Sec. III. All results in this Section are obtained for nanotubes of $R = 10$ nm.

A. Streaming current

Figure 2 shows the streaming current as a function of applied pressure gradient. The calculations are made for several hydrophobic nanotubes of the same radius $R = 10$ nm, surface charge and slip length, but different μ, computed for two concentrations of salt, $c_\infty = 10^{-5}$ mol/L and $c_\infty = 10^{-1}$ mol/L which corresponds to $\lambda_D \simeq 100$ nm and 1 nm, i.e. to the regimes of thin and thick cylinder. The fixed $\ell_{GC} = 5$ nm corresponds to a surface charge density $\sigma \simeq 7.3$ mC/m^2. The response is always linear, and the slope of the straight lines is invoked to find the electro-osmotic mobility M_e that depends on c_∞. The computed data show that for nanotubes of the same μ a larger J is observed at lower concentration, but a four orders of magnitude increase in c_∞ reduce the streaming current only slightly. However, on reducing μ from 0.75 down to 0.25 the streaming current is significantly suppressed. Once M_e is known, we can determine the value of ζ. Calculations from Eq. (24) show that the numerical results (from top to bottom) in Fig. 2 correspond to $\zeta \simeq 4.7, 4.2$ and 2.2. Also included in Fig. 2 are the streaming currents calculated analytically using ζ given by (25) with ζ_0 obtained for the thin and thick cylinder limits (Eqs.(43) and (45)). We see that with these parameters Eq. (43) provides an excellent fit to numerical results, but Eq. (45) slightly overestimates the results. It must be remembered that this is a first-order calculation only, and given the simplifications made we do not expect it to be very accurate.

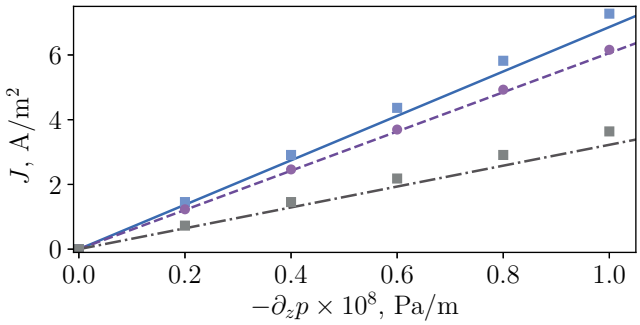

FIG. 2. Streaming current density J vs. pressure drop $\partial_z p$ computed for hydrophobic cylinders of $R = 10$ nm, $b = 10$ nm and $\ell_{GC} = 5$ nm. The solid line shows numerical results obtained using $\mu = 0.75$ and $c_\infty = 10^{-5}$ mol/L. The dashed line is computed for $\mu = 0.75$ and $c_\infty = 10^{-1}$ mol/L. The dash-dotted line is computed for $c_\infty = 10^{-5}$ mol/L and $\mu = 0.25$. Circles and squares show calculations using ζ_0 given by Eqs.(43) and (45), respectively.

We now turn to zeta potential of nanotubes. The main issue we address is how to enhance ζ by generating a slip velocity at the surface and by tuning the salt concentration. Figure 3 includes ζ computed as a function of c_∞. Note that varying c_∞ from 10^{-6} to 10^{-1} mol/L is equivalent to the range of R/λ_D from 0.032 to 10.3. In this calculations we keep $\ell_{GC} = 5$ nm fixed, so that ϕ_s varies with salt, but the ratio $b/\ell_{GC} = 2$ remains constant, i.e. independent on c_∞. The computed ϕ_s is

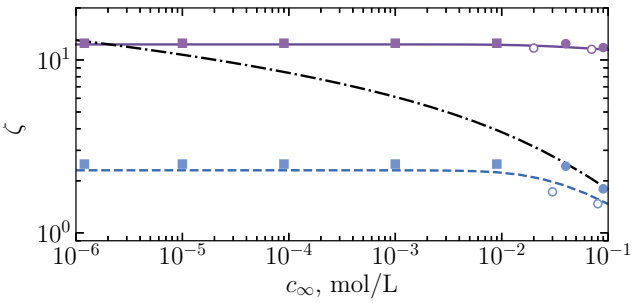

FIG. 3. Zeta potential as a function of c_∞ computed for cylindrical channels of $R = 10$ nm, $\ell_{GC} = 5$ nm, $b = 10$ nm using $\mu = 0.5$ (solid curve) and 0 (dashed curve). The surface potential ϕ_s is shown by dash-dotted curve. Filled circles show ζ calculated using ζ_0 predicted by Eq.(43), open circles are calculated using ζ_0 given by Eq.(B8). Squares are obtained using ζ_0 calculated from Eq.(45).

also included in Fig. 3. It can be seen that on increasing c_∞ it reduces, but never becomes small. The calculations of ζ are made using $\mu = 0.5$ and 0. As discussed above, in the latter case of fully mobile surface charges $\zeta = \zeta_0$, although the hydrodynamic slip length is finite. For the thin nanotubes ζ does not depend on salt and takes its maximal (constant) value. When nanotubes become thick, ζ begins to decrease with c_∞. It can be seen that when $\mu = 0$ the surface potential is always larger than $\zeta = \zeta_0$, but at $\mu = 0.5$ the zeta potential is significantly amplified by hydrodynamic slippage and in the sufficiently concentrated solutions ζ dramatically exceeds ϕ_s. The numerical data are compared with the analytical calculations in which ζ_0 is evaluated using Eqs.(43) (thick nanotubes, $c_\infty \simeq 10^{-1}$ mol/L) or (45) (thin nanotubes, $c_\infty \leq 10^{-2}$ mol/L). The fits are quite good, but there is some discrepancy. The analytical equations overestimate the exact numerical results, which is the consequence of an assumption $\overline{\phi} \simeq 0$ (see Sec. III A). Similar fits for thick nanotubes made using a next order approximation, Eq.(B8), would make an improvement to the fit, but slightly underestimate the numerical results.

The amplification of the zeta potential relative to ζ_0 is illustrated in Fig. 4, where the data are reproduced from Fig. 3. With these parameters ζ of the hydrophobic channel is amplified in ca. 3.5 times in dilute solutions, where $\lambda_D \geq R$. In more concentrated solutions (of small λ_D) ζ/ζ_0 begins to rapidly augment with c_∞ to larger values. It is instructive to compare these results with a calculation of ζ/ϕ_s, also included in Fig. 4. This ratio increases with c_∞ strictly monotonically and is always lower than ζ/ζ_0. When $c_\infty \leq 10^{-3}$ mol/L, ζ/ϕ_s is smaller than unity, but then ζ exceeds ϕ_s. This is especially well seen in Fig. 3. Also included in Fig. 4 are the theoretical results for ζ/ζ_0 obtained from Eqs.(47) and (48). The theoretical predictions provide a good qualitative agreement with the numerical data, but show smaller amplification of the zeta potential. An obvious explanation for this discrepancy is the neglected average potential of the nanotube. Indeed, Eq.(B8) that takes into account a non-zero $\overline{\phi}$ for the high concentration branch in Fig. 4 provides a better match to the numerical data.

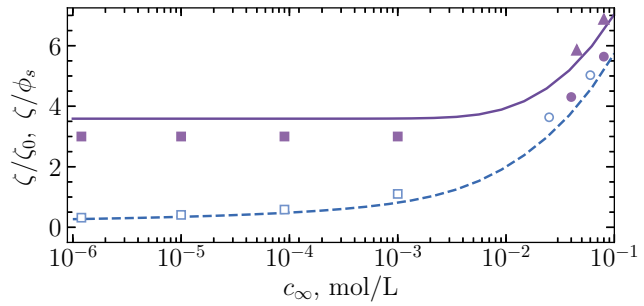

FIG. 4. ζ/ζ_0 (solid curve) and ζ/ϕ_s (dashed curve) computed as a function of c_∞ for cylindrical channels of $R = 10$ nm, $\ell_{GC} = 5$ nm, $b = 10$ nm, and $\mu = 0.5$. Filled circles and squares are obtained from (47) and (48), respectively. Filled triangles show ζ/ζ_0 calculated using ζ_0 given by (B8). Filled circles and squares are calculations of ζ/ϕ_s with ϕ_s obtained from (B4) and (B13).

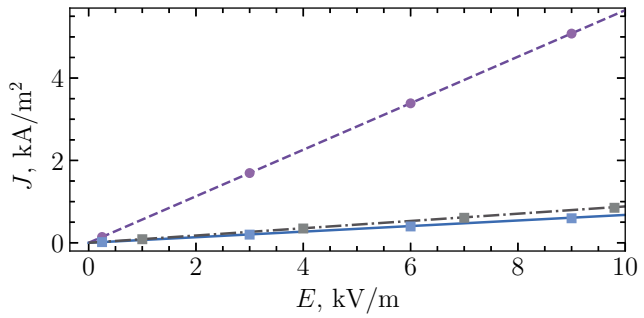

FIG. 5. Conductivity current density J vs. electric field E computed for the same nanotubes and c_∞ as in Fig. 2. Symbols show J calculated using Ohm's law with K given by Eq.(40) and ΔK determined from (42). The circles correspond to K_0 calculated from (49). The squares are calculations using K_0 given by (50).

If similar fits are made to a ζ/ϕ_s curve, as shown in Fig. 4, it is found that the agreement of analytical theory that invokes Eqs.(B4) and (B13) for ϕ_s with numerical results is very good.

B. Electrical conductivity

Next, we turn to the mean conductivity of the channel K. Figure 5 shows a current-voltage response ($J-E$) computed for the same nanotubes and electrolyte concentrations as in Fig. 2. The numerical examples show that J is largest for $c_\infty = 10^{-1}$ mol/L. The mean electric current density computed using $c_\infty = 10^{-5}$ mol/L is ca. an order of magnitude smaller. The slope of the $J-E$ straight line is invoked to find the conductivity K at given c_∞. Therefore, we conclude that numerical data at $c_\infty = 10^{-5}$ mol/L shows conductivity that is an order of magnitude smaller than this computed using $c_\infty = 10^{-1}$ mol/L. Meantime, the bulk conductivity is four order of magnitude smaller as follows from Eq.(34). These numerical data are compared with the above theoretical results. The mean

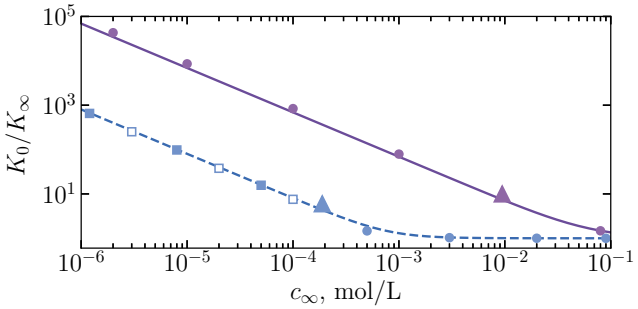

FIG. 6. K_0/K_∞ as a function of c_∞ computed for nanotubes of $R = 10$ nm, using $\ell_{GC} = 1$ and 50 nm (from top to bottom). Circles show calculations using K_0 calculated from Eq.(49). Filled and open squares are obtained using K_0 from Eqs.(50) and (51). The big triangles mark the points of $\ell_{Du}/R = 1$.

conductivity of the nanotube is calculated from Eq.(40). To calculate K_0 in this equation in the case of $c_\infty = 10^{-1}$ mol/L we use Eq.(49) since λ_D/R is small. The calculation of K_0 at $c_\infty = 10^{-5}$, where λ_D/R is large, are performed using (50). For both concentrations to obtain ΔK we, of course, employ Eq.(42). Once K is known, J can be found employing Ohm's law. Theoretical results are included in Fig. 5. It can be seen that the numerical data sets are very well fitted by analytical equations.

To examine the significance of deviations from the bulk conductivity more closely, in Fig. 6 we plot K_0/K_∞ as a function of c_∞. The calculations are made using $\ell_{GC} = 1$ and 50 nm. The conductivity of hydrophilic nanotubes, K_0, can be very large (nearly five orders of magnitude larger than K_∞) if it is highly charged ($\ell_{GC} = 1$ nm), but even for $\ell_{GC} = 50$ nm we observe ca. three orders of magnitude enhancement, provided that an electrolyte solution is extremely dilute. On increasing c_∞ (reducing λ_D and ℓ_{Du}), K_0/K_∞ first decays linearly in this log-log plot indicating that $K_0/K_\infty \propto c_\infty^{-1}$. However, on increasing c_∞ further K_0/K_∞ begins to reduce weaker (down to 1). We have marked with triangles the points of $\ell_{Du}/R = 1$ and one can see that this branch for both curves occurs in the vicinity of these points. The upper curve that corresponds to a highly charged cylinder is well fitted using K_0 given by Eq.(49) indicating that the nanotube effectively behaves as thick even when λ_D/R is large. The curve for the weakly charged nanotube is well described using K_0 calculated from Eq.(50) when c_∞ is below 10^{-4} mol/L. The use of (51) makes practically no difference to the fit, as expected. At concentrations $c_\infty \geq 10^{-3}$ mol/L the weakly charged nanotube is effectively thick and the numerical data are well fitted if K_0 given by (49) is employed.

The mean conductivity of the nanotubes can be amplified by the slippage effect. This is illustrated in Fig. 7, where the amplification of the mean conductivity is calculated using $\mu = 0.5$ (a half of surface charges is mobile) and a moderate slip length $b = 10$ nm. For these examples we use $\ell_{GC} = 1$ and 50 nm, the same as in Fig. 6. It can be seen, that for low concentrations ($\ell_{Du}/R \geq 1$) the conductivity amplifica-

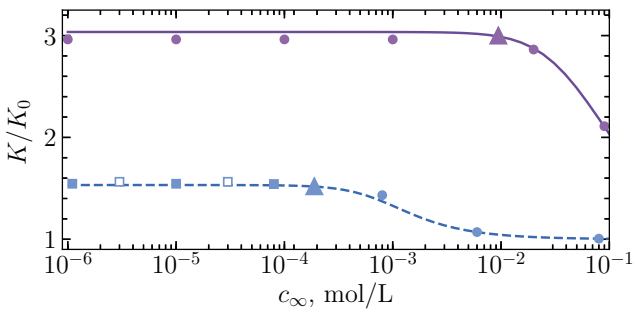

FIG. 7. The conductivity amplification K/K_0 as a function of c_∞ obtained for the same nanotubes as in Fig. 6, but with $b = 10$ nm, and $\mu = 0.5$. Filled symbols are obtained using K_0 from Fig. 6 and K calculated from (40). Open squares show calculations from Eq.(52). The big triangles mark the points of $\ell_{Du}/R = 1$.

tion due to slip, K/K_0, is independent on salt and takes its largest value. For a highly charged nanotube ($\ell_{GC} = 1$ nm) the slippage increase the conductivity by a factor of ca. 3, but for a weakly charged cylinder the enhancement is low with these papameters. When ℓ_{Du}/R becomes smaller than unity, the value of K/K_0 decreases with salt. It is well seen that for a curve calculated using $\ell_{GC} = 50$ nm $K \simeq K_0$ when $c_\infty \geq 10^{-2}$ mol/L. In other words, there is no conductivity amplification due to slippage. However, a highly charged nanotube ($\ell_{GC} = 1$ nm) shows the enhancement of the mean conductivity in ca. 2 times even when $c_\infty = 10^{-1}$ mol/L. The results of theoretical calculations are also shown in Fig. 7. The theoretical data for K_0 of Fig. 6 are reproduced and summed up with ΔK given by (42) to obtain K. Calculated values of K/K_0 fit very well the numerical curves. We have also verified Eq.(52). As predicted, it represents a sensible approximation for K/K_0 if $\ell_{Du}/R \geq 1$ and $\lambda_D/\ell_{GC} \leq 1$. Indeed, the plateau branch of the numerical curve obtained using $\ell_{GC} = 50$ nm is well fitted by Eq.(52).

V. CONCLUSION

We have presented a theory describing the transport of ions in hydrophobic nanotubes with the constant surface charge density. The electro-hydrodynamic boundary condition [31] is imposed at the hydrophobic wall, which assumes that the surface demonstates a hydrodynamic slippage and some portion of the adsorbed surface charges can migrate relative to fluid by reacting to the applied electric field (but not to the hydrodynamic tangential stress). Numerical solutions are presented and fully validate our analysis. These results are directly relevant for enhanced streaming and conductivity currents in carbon and boron nitride nanotubes, which are currently the area of very active research, as well as for conventional nanoporous membranes.

The main results of our work can be summarized as follows. We have proven that when the electro-hydrodynamic boundary condition is applied the Onsager relations hold provided the adsorbed surface ions are transferred in a pressure-driven flow with the slip velocity of liquid. Namely, we have derived general expressions for elements of the 2×2 mobility matrix, Eq.(10), and demonstrated that the off-diagonal coefficients are equal if the electro-hydrodynamic boundary condition, Eq.(14), is imposed and provided Eq.(21) is valid. These expressions include some mean electrostatic functions, which we have calculated analytically for two specific regimes (of thin and thick nanotubes). Importantly, these regimes are defined not by just λ_D/R, but also controlled by the value of λ_D/ℓ_{GC}, i.e. effective charge of the walls. We have then derived simple analytical approximations for the electro-osmotic mobility and mean conductivity in these two regimes. Our results show that qualitative features of the electrosmotic mobility and conductivity curves for cylinders are the same as for slits, but there is some important quantitative difference due to different expressions for electrostatic functions. We have also given a novel interpretation of the zeta potential of nanotubes.

Our results open strategies to tune the ion transport in nanotubes via a modification of their walls and, vice versa, to probe surface properties by measuring the streaming or conductivity currents. Our quantitative results can be improved by performing more accurate calculations of the central (axis) potential. This remains a challenging mathematical problem and a subject of future research. Other fruitful directions would be to extend the results for so-called charge regulation surfaces and for systems, where both pressure drop and electric field are applied simultaneously. The latter calculations are now straightforward and can be done by using the proven Onsager relations.

ACKNOWLEDGMENTS

This work was supported by the Ministry of Science and Higher Education of the Russian Federation.

DATA AVAILABILITY

The data that support the findings of this study are available within the article.

Appendix A: Mobility of ions in dilute 1:1 electrolyte solutions

In general case, the electrophoretic mobility of ions reduces with the concentration of salt. If $\mathscr{R} \ll \lambda_D$, the mobilities of monovalent ions can be approximately described by the Hückel formula [45]

$$m \simeq \frac{e}{6\pi\eta\mathscr{R}}\left(1 - \frac{\mathscr{R}}{\lambda_D}\right) \tag{A1}$$

Using (6) this can be rewritten as

$$m \simeq \frac{e}{6\pi\eta\mathscr{R}}\left(1 - \frac{\mathscr{R}\sqrt{c_\infty}}{0.305}\right) \tag{A2}$$

This expression shows that the mobility at infinite dilution represents its upper possible limit. The deviations from this ideal mobilty in dilute solutions do not depend on the ion radius and scale with $c_\infty^{1/2}$. Thus, Eq.(A2) is functionally equivalent to the Kohlrausch empirical model [46].

It follows from (A2) that at $c_\infty = 10^{-2}$ mol/L the decrease in the mobilities of ions of $\mathscr{R} = 0.3$ nm compared to those at an infinite dilution is less than 10%. Concequently for solutions of $c_\infty \leq 10^{-2}$ mol/L (where $\mathscr{R}/\lambda_D$ is small), this effect can safely be neglected. At larger concentrations the analysis based on an upper limit of ion mobilities becomes quite approximate. Nevertheless, it provides us with some guidance. As a side note, at our largest concentration $c_\infty = 10^{-1}$ mol/L the use of Eq.(A1) would also represent too rough an approximation since $\mathscr{R}/\lambda_D \simeq 0.3$.

Appendix B: Derivation of electrostatic equations

Expressions for the mean osmotic pressure $\overline{\cosh\phi}$ and for the mean square derivative of the electrostatic potential $\overline{(\phi')^2}$, which is the measure of the electrostatic field energy (per unit area), can be derived similar to [35]. First integration of Eq.(5) from the axis ($r = 0$) to an arbitrary r gives

$$\lambda_D^2 \left(\frac{d\phi}{dr}\right)^2 = 2\cosh\phi - \frac{4}{r^2}\int_0^r r\cosh\phi\, dr \qquad \text{(B1)}$$

Applying boundary condition (7) then yields

$$\overline{\cosh\phi} = \cosh\phi_s - \frac{2\ell_{Du}}{\ell_{GC}}. \qquad \text{(B2)}$$

The expression (B2) is exact and valid for any channel thickness and surface charge/potential. In Fig. 8 we present numerical solutions to validate Eq.(B2) and illustrate the variation of $\overline{\cosh\phi}$ in response to λ_D/ℓ_{GC} and λ_D/R.

Note that from (5) and (7) it follows that

$$\overline{\sinh\phi} = \frac{4\ell_{Du}}{R} \qquad \text{(B3)}$$

1. Thick channel

For a single wall or an infinitely large cylinder the relation between the surface potential and charge is given by the Grahame equation

$$\phi_s = 2\,\mathrm{arsinh}\left(\frac{\lambda_D}{\ell_{GC}}\right) \qquad \text{(B4)}$$

In Fig. 9 we plot ϕ_s as a function of λ_D/ℓ_{GC}. It can be seen that Eq.(B4) remains very accurate for a thick channel and even when $\lambda_D/R = O(1)$ provided λ_D/ℓ_{GC} is large.

Substituting (B4) into (B2) one obtains $\overline{\cosh\phi} = 1$, which is equivalent to $\overline{\phi} = 0$ and $\overline{(\phi')^2} = 0$. However, this result holds only if $R \to \infty$. The data presented in Fig. 8 show that $\overline{\cosh\phi}$ is well above unity at finite λ_D/ℓ_{GC}, even for a thick channel, indicating that $\overline{\phi} \neq 0$.

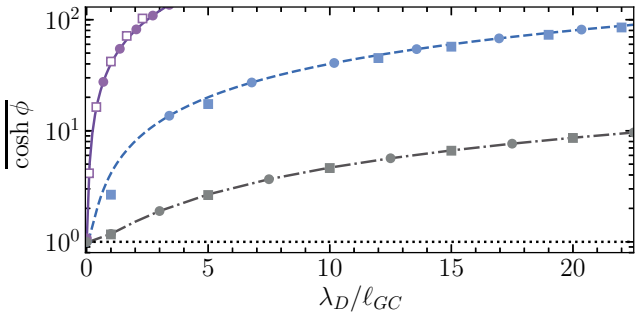

FIG. 8. $\overline{\cosh\phi}$ as a function of λ_D/ℓ_{GC} computed for cylindrical channels of $R = 10$ nm with fixed $\lambda_D = 100$ nm (solid curve), $\lambda_D = 10$ (dashed curve), and $\lambda_D = 1$ (dash-dotted curve). The dotted line indicates $\overline{\cosh\phi} = 1$. Circles show predictions of Eq.(B2). Squares are obtained using Eqs.(B9) and (B15).

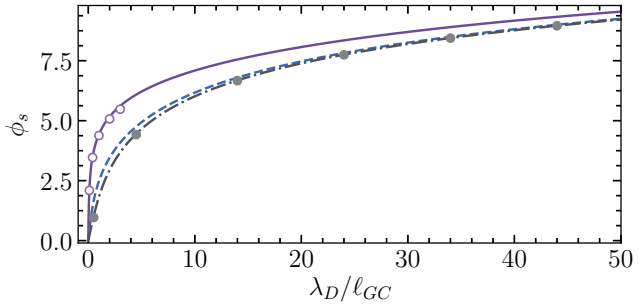

FIG. 9. Surface potential, ϕ_s, as a function of λ_D/ℓ_{GC} calculated numerically using $R/\lambda_D \simeq 0.1$, 1, and 10 (from top to bottom). Filled and open circles show calculations from Eqs. (B4) and (B13).

The calculation of $\overline{\phi}$ represents a challenge for a cylindrical geometry and we leave this for a future research. However, when the nanotube is weakly charged, $\phi_s \leq 1$, one can linearize Eq. (5):

$$\frac{1}{r}\frac{d}{dr}\left(r\frac{d\phi}{dr}\right) \simeq \lambda_D^{-2}\phi \qquad \text{(B5)}$$

Integrating the above equation (B5) we obtain the potential profile:

$$\phi \simeq \frac{2\lambda_D}{\ell_{GC}}\frac{I_0(r/\lambda_D)}{I_1(R/\lambda_D)}, \qquad \text{(B6)}$$

where I_0 and I_1 are the modified Bessel functions. The average potential is then

$$\overline{\phi} \simeq \frac{4\ell_{Du}}{R} \qquad \text{(B7)}$$

It follows from (B4) that for weakly charged surfaces $\phi_s \simeq 2\lambda_D/\ell_{GC}$. Using (26) we then obtain

$$\zeta_0 \simeq \frac{2\lambda_D}{\ell_{GC}}\left(1 - \frac{2\lambda_D}{R}\right) \qquad \text{(B8)}$$

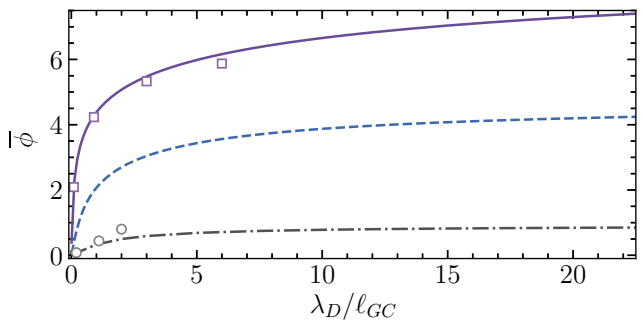

FIG. 10. $\overline{\phi}$ as a function of R/λ_D computed for cylindrical channels of $R = 10$ nm with fixed $\phi_s = 5$ and 1 (from top to bottom). Squares are obtained using Eq. (B14). Circles show predictions of linear theory Eq. (B7).

The numerical data presented in Fig. 10 confirm the validity of Eq.(B7) at $\lambda_D/\ell_{GC} \leq 1$ but show smaller $\overline{\phi}$ than this theoretical prediction when λ_D/ℓ_{GC} becomes larger. A calculation of the average potential and its effect on the zeta potential in the case of a highly charged thick nanotube remains very difficult and well beyond the scope of this paper. Nevertheless, we see that at large λ_D/ℓ_{GC} the surface potential (see Fig. 9) is much higher than $\overline{\phi}$, so that the later can be neglected in the first-order calculations. Clearly, given this simplification we do not expect the calculations of the zeta potential to be very accurate.

It is naturally to assume that corrections to $\overline{\cosh\phi}$ and $\overline{(\phi')^2}$ are proportional to the ratio of the EDL length to the channel area. Performing similar to described in [35] calculations we obtain

$$\overline{\cosh\phi} \simeq 1 + \frac{4\lambda_D}{R}\left(\sqrt{1+\frac{\ell_{Du}}{\ell_{GC}}} - 1\right), \tag{B9}$$

and

$$\overline{(\phi')^2} \simeq \frac{8}{R\lambda_D}\left(\sqrt{1+\frac{\ell_{Du}}{\ell_{GC}}} - 1\right), \tag{B10}$$

Note that it follows then that these functions are related as

$$\overline{\cosh\phi} \simeq 1 + \frac{\lambda_D^2\overline{(\phi')^2}}{2}. \tag{B11}$$

Calculations from (B9) are shown in Fig. 8. It can be seen that Eq.(B9) gives a good match to the numerical data for thick nanotubes, and can even be used when $R \simeq \lambda_D$.

2. Thin channel

In the thin channel limit, $R/\lambda_D \ll 1$, the distribution of a potential in the channel is approximately given by the parabola [43]

$$\phi(r) = \phi_s + \frac{\sinh\phi_s}{4\lambda_D^2}\left(r^2 - R^2\right). \tag{B12}$$

The relation between the surface potential and adsorbed charge reads [43]:

$$\phi_s = \operatorname{arsinh}\frac{4\ell_{Du}}{R}. \tag{B13}$$

The calculations from Eq.(B13) are included in Fig. 9. It can be seen that (B13) is accurate only when λ_D/ℓ_{GC} is small enough.

It follows then that the average potential is given by

$$\overline{\phi} \simeq \phi_s - \frac{R^2\sinh\phi_s}{8\lambda_D^2} \simeq \operatorname{arsinh}\frac{4\ell_{Du}}{R} - \frac{R}{2\ell_{GC}} \tag{B14}$$

The calculation from Eq.(B14) are compared with numerical results in Fig. 10. The fit is quite good for $\lambda_D/\ell_{GC} \leq 3$, but at larger λ_D/ℓ_{GC} there is some discrepancy, and the average potential is higher than predicted by Eq.(B14).

By direct integration of Eq. (B12) using (B2) and (B13) we can easily derive

$$\overline{\cosh\phi} \simeq \sqrt{1+\left(\frac{4\ell_{Du}}{R}\right)^2} - \frac{2\ell_{Du}}{\ell_{GC}} \tag{B15}$$

and

$$\overline{(\phi')^2} \simeq \frac{2}{\ell_{GC}^2} \tag{B16}$$

[1] R. B. Schoch, J. Han, and P. Renaud, Transport phenomena in nanofluidics, Rev. Mod. Phys. **80**, 839 (2008).
[2] L. Bocquet and E. Charlaix, Nanofluidics, from bulk to interfaces, Chem. Soc. Rev. **39**, 1073 (2010).
[3] W. Sparreboom, A. van den Berg, and J. C. Eijkel, Principles and applications of nanofluidic transport, Nature nanotechnology **4**, 713 (2009).
[4] H. Daiguji, Ion transport in nanofluidic channels, Chemical Society Reviews **39**, 901 (2010).
[5] B. M. Venkatesan and R. Bashir, Nanopore sensors for nucleic acid analysis, Nature nanotechnology **6**, 615 (2011).
[6] K. Xiao, L. Jiang, and M. Antonietti, Ion transport in nanofluidic devices for energy harvesting, Joule **3**, 2364 (2019).
[7] Z. Hao, Q. Zhang, X. Xu, Q. Zhao, C. Wu, J. Liu, and H. Wang, Nanochannels regulating ionic transport for boosting electrochemical energy storage and conversion: a review, Nanoscale **12**, 15923 (2020).
[8] R. J. Hunter, *Zeta Potential in Colloid Science: Principles and Applications*, Vol. 2 (Academic press, 2013).
[9] B. J. Kirby and E. F. Hasselbrink Jr, Zeta potential of microflu-

idic substrates: 1. Theory, experimental techniques, and effects on separations, Electrophoresis **25**, 187 (2004).
[10] S. Kamble, S. Agrawal, S. Cherumukkil, V. Sharma, R. V. Jasra, and P. Munshi, Revisiting zeta potential, the key feature of interfacial phenomena, with applications and recent advancements, ChemistrySelect **7**, e202103084 (2022).
[11] D. Stein, M. Kruithof, and C. Dekker, Surface-charge-governed ion transport in nanofluidic channels, Phys. Rev. Lett. **93**, 035901 (2004).
[12] R. B. Schoch, H. van Lintel, and P. Renaud, Effect of the surface charge on ion transport through nanoslits, Phys. Fluids **17**, 100604 (2005).
[13] A. Siria, P. Poncharal, A.-L. Biance, R. Fulcrand, X. Blase, S. T. Purcell, and L. Bocquet, Giant osmotic energy conversion measured in a single transmembrane boron nitride nanotube, Nature **494**, 455 (2013).
[14] S. Balme, F. Picaud, M. Manghi, J. Palmeri, M. Bechelany, S. Cabello-Aguilar, A. Abou-Chaaya, P. Miele, E. Balanzat, and J. M. Janot, Ionic transport through sub-10 nm diameter hydrophobic high-aspect ratio nanopores: experiment, theory and simulation, Sci. Rep. **5**, 10135 (2015).
[15] H. Xie, T. Saito, and M. A. Hickner, Zeta potential of ion-conductive membranes by streaming current measurements, Langmuir **27**, 4721 (2011).
[16] S. Salgin, U. Salgin, and N. Soyer, Streaming potential measurements of polyethersulfone ultrafiltration membranes to determine salt effects on membrane zeta potential, Int. J. Electrochem. Sci **8**, 4073 (2013).
[17] Y. Xie, L. Wang, M. Jin, Y. Wang, and J. Xue, Non-linear streaming conductance in a single nanopore by addition of surfactants, Applied Physics Letters **104**, 033108 (2014).
[18] S. Chen, H. Dong, and J. Yang, Surface potential/charge sensing techniques and applications, Sensors **20**, 1690 (2020).
[19] O. I. Vinogradova, Slippage of water over hydrophobic surfaces, Int. J. Miner. Process. **56**, 31 (1999).
[20] O. I. Vinogradova and A. V. Belyaev, Wetting, roughness and flow boundary conditions, J. Phys.: Condens. Matter **23**, 184104 (2011).
[21] C. Cottin-Bizonne, B. Cross, A. Steinberger, and E. Charlaix, Boundary slip on smooth hydrophobic surfaces: Intrinsic effects and possible artifacts, Phys. Rev. Lett. **94**, 056102 (2005).
[22] O. I. Vinogradova and G. E. Yakubov, Dynamic effects on force measurements. 2. Lubrication and the atomic force microscope, Langmuir **19**, 1227 (2003).
[23] L. Joly, C. Ybert, and L. Bocquet, Probing the nanohydrodynamics at liquid-solid interfaces using thermal motion, Phys. Rev. Lett. **96**, 046101 (2006).
[24] O. I. Vinogradova, K. Koynov, A. Best, and F. Feuillebois, Direct measurements of hydrophobic slipage using double-focus fluorescence cross-correlation, Phys. Rev. Lett. **102**, 118302 (2009).
[25] V. M. Muller, I. P. Sergeeva, V. D. Sobolev, and N. V. Churaev, Boundary effects in the theory of electrokinetic phenomena, Colloid J. USSR **48**, 606 (1986).
[26] N. V. Churaev, J. Ralston, I. P. Sergeeva, and V. D. Sobolev, Electrokinetic properties of methylated quartz capillaries, Adv. Colloid Interface Sci. **96**, 265 (2002).
[27] M. C. Audry, A. Piednoir, P. Joseph, and E. Charlaix, Amplification of electro-osmotic flows by wall slippage: Direct measurements on OTS-surfaces, Faraday Discuss. **146**, 113 (2010).
[28] S. Dehe, B. Rofman, M. Bercovici, and S. Hardt, Electro-osmotic flow enhancement over superhydrophobic surfaces, Physical Review Fluids **5**, 053701 (2020).
[29] S. Levine, J. R. Marriott, and K. Robinson, Theory of electrokinetic flow in a narrow parallel-plate channel, Journal of the Chemical Society, Faraday Transactions 2: Molecular and Chemical Physics **71**, 1 (1975).
[30] D. Andelman, Soft condensed matter physics in molecular and cell biology (CRC Press, Boca Raton, 2006) Chap. 6. Introduction to Electrostatics in Soft and Biological Matter, 1st ed.
[31] S. R. Maduar, A. V. Belyaev, V. Lobaskin, and O. I. Vinogradova, Electrohydrodynamics near hydrophobic surfaces, Phys. Rev. Lett. **114**, 118301 (2015).
[32] B. Grosjean, M.-L. Bocquet, and R. Vuilleumier, Versatile electrification of two-dimensional nanomaterials in water, Nat. Com. **10**, 1656 (2019).
[33] T. Mouterde and L. Bocquet, Interfacial transport with mobile surface charges and consequences for ionic transport in carbon nanotubes, Eur. Phys. J. E **41**, 148 (2018).
[34] E. Mangaud, M.-L. Bocquet, L. Bocquet, and B. Rotenberg, Chemisorbed vs physisorbed surface charge and its impact on electrokinetic transport: Carbon vs boron nitride surface, The Journal of Chemical Physics **156**, 044703 (2022).
[35] O. I. Vinogradova, E. F. Silkina, and E. S. Asmolov, Enhanced transport of ions by tuning surface properties of the nanochannel, Phys. Rev. E **104**, 035107 (2021).
[36] C. L. Rice and R. Whitehead, Electrokinetic flow in a narrow cylindrical capillary, J. Phys. Chem. **69**, 4017 (1965).
[37] S. Levine, J. Marriott, G. Neale, and N. Epstein, Theory of electrokinetic flow in fine cylindrical capillaries at high zeta-potentials, Journal of Colloid and Interface Science **52**, 136 (1975).
[38] P. M. Biesheuvel and M. Z. Bazant, Analysis of ionic conductance of carbon nanotubes, Phys. Rev. E **94**, 050601 (2016).
[39] P. Peters, R. Van Roij, M. Z. Bazant, and P. Biesheuvel, Analysis of electrolyte transport through charged nanopores, Phys. Rev. E **93**, 053108 (2016).
[40] Y. Uematsu, R. R. Netz, L. Bocquet, and D. J. Bonthuis, Crossover of the power-law exponent for carbon nanotube conductivity as a function of salinity, The Journal of Physical Chemistry B **122**, 2992 (2018).
[41] J. Catalano, R. G. H. Lammertink, and P. M. Biesheuvel, Theory of fluid slip in charged capillary nanopores, arXiv:1603.09293 (2016).
[42] Y. Green, Ion transport in nanopores with highly overlapping electric double layers, J. Chem. Phys. **154**, 084705 (2021).
[43] E. F. Silkina, E. S. Asmolov, and O. I. Vinogradova, Electro-osmotic flow in hydrophobic nanochannels, Phys. Chem. Chem. Phys. **21**, 23036 (2019).
[44] J. N. Israelachvili, *Intermolecular and Surface Forces*, 3rd ed. (Academic Press, 2011).
[45] E. Huckel, Die Kataphorese der Kugel, Physikalische Zeitschrift **25**, 204 (1924).
[46] F. Kohlrausch, Ueber den stationären Temperaturzustand eines elektrisch geheizten Leiters, Annalen der Physik **306**, 132 (1900).